Electronic Supplementary Material (ESI) for Journal of Materials Chemistry A.

$R-$$Nb_2O_5$ has an 'idealized' V_2O_5 structure and Wadsley$-$Roth-like structural stability during Li-ion battery cycling

Kausturi Parui, Alexander D. Lee, Shornam Gandhi, and Megan M. Butala*

Department of Materials Science and Engineering, University of Florida, Gainesville, FL 32611

E-mail: mbutala@ufl.edu

Supporting Information

Additional information on Rietveld Refinements

Table S1: R−Nb_2O_5 unit cell and structure parameters from the Rietveld refinement of neutron diffraction data from POWGEN (Spallation Neutron Source, Oak Ridge National Laboratory) using Topas Academic v7.[1] Peak breadth and reflection-character-dependent broadening were modeled using crystallite size (CS_G and CS_L parameters), March-Dollase preferred orientation (spherical harmonics, order 8), and strain (strain_G, strain_L).

R−Nb_2O_5, $A2/m$ (No. 12, unique setting b)					
R_p = 8.99, R_{wp} = 7.85					
a = 3.9752(6) Å b = 3.8233(3) Å c = 12.7064(19) Å β = 90.603(13)°					
V_{uc} = 193.11(4) Å^3					
Atom	x	y	z	occ	B_{eq}
Nb	0.0749(17)	0	0.1547(5)	1	0.48(7)
O	0.012(2)	0	0.6757(5)	1	0.33(5)
O	0.504(2)	0	0.1514(6)	1	0.33(5)
O	0	0	0	1	0.33(5)

Table S2: R−Nb_2O_5 unit cell and structure parameters from the Rietveld refinement of 11-BM XRD using Topas Academic v7.[1] Peak breadth and reflection-character-dependent broadening were modeled using crystallite size (CS_G and CS_L parameters), March-Dollase preferred orientation (spherical harmonics, order 8), and strain (strain_G, strain_L).

R−Nb_2O_5, $A2/m$ (No. 12, unique setting b)					
R_p = 14.28, R_{wp} = 18.14					
a = 3.9833(3) Å b = 3.8365(16) Å c = 12.7541(7) Å β = 90.603(7)°					
V_{uc} = 194.901(19) Å^3					
Atom	x	y	z	occ	B_{eq}
Nb	0.0532(10)	0	0.14707(19)	1	2.00(9)
O	−0.101(5)	0	0.6771(11)	1	0.10(19)
O	0.472(4)	0	0.1482(11)	1	0.10(19)
O	0	0	0	1	0.10(19)

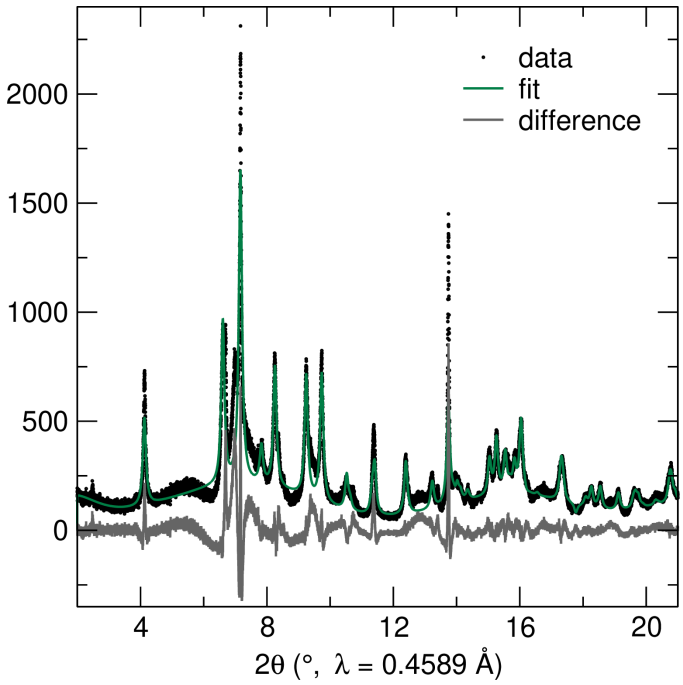

Figure S1: Rietveld refinement against high-resolution synchrotron XRD data for as-prepared $R-Nb_2O_5$ shows good agreement between the measured and calculated patterns. The largest differences occur in regions with diffuse scattering, as well as for two reflections that are underestimated in the calculated data.

Table S3: Unit cell and structure parameters for the Nb−O framework for lithiated $R-Nb_2O_5$ (discharged to 0.5 V) from the Rietveld refinement of 11-BM XRD using Topas Academic v7.[1] Peak breadth and reflection-character-dependent broadening were modeled using crystallite size (CS_G and CS_L parameters), March-Dollase preferred orientation (spherical harmonics, order 8), and strain (strain_G, strain_L).

$Li_3Nb_2O_5$, $A2/m$ (No. 12, unique setting b)					
$R_p = 8.38$, $R_{wp} = 10.72$					
$a = 3.94788(19)$ Å	$b = 4.04267(15)$ Å	$c = 12.6633(7)$ Å	$\beta = 90.0034(10)°$		
$V_{uc} = 202.107(17)$ Å^3					
Atom	x	y	z	occ	B_{eq}
Nb	−0.0039(4)	0	0.15543(15)	1	0.10(13)
O	0.010(19)	0	0.6791(5)	1	0.93(17)
O	0.510(2)	0	0.1523(6)	1	0.93(17)
O	0	0	0	1	0.93(17)

Table S4: Unit cell and structure parameters for the Nb−O framework for the *ex situ* product after one discharge and charge cycle of R−Nb_2O_5 (discharged to 0.5 V, charged to 2.5 V). Values were determined through Rietveld refinement of 11-BM XRD using Topas Academic v7.[1] Peak breadth and reflection-character-dependent broadening were modeled using crystallite size (CS_G and CS_L parameters), March-Dollase preferred orientation (spherical harmonics, order 8), and strain (strain_G, strain_L).

$Li_1Nb_2O_5$, $A2/m$ (No. 12, unique setting b)					
R_p = 9.42, R_{wp} = 11.9					
a = 3.9313(3) Å	b = 4.0058(2) Å	c = 12.6987(10) Å			
β =89.966(11)°	V_{uc} = 199.98(2) Å^3				
Atom	x	y	z	occ	B_{eq}
Nb	−0.010(3)	0	0.15421(17)	1	0.10(14)
O	0.010(19)	0	0.6791(5)	1	0.10(18)
O	0.510(2)	0	0.1523(6)	1	0.10(18)
O	0	0	0	1	0.10(18)

Additional cycling data

In Swagelok cells with loose powder cathodes, there was a more significant difference (Fig. S2) between the first and following discharge profiles. Even though the capacity was higher for lower potential limits below 1 V, the capacity faded more rapidly than in coin cells with cast cathode films.

Additionally, R−Nb_2O_5 exhibits good stability and reversibility at faster rates of cycling, as evident from the coin cells cycled at faster rates of $C/10$ (Fig. S3) and $1C$ (Fig. S4). This high reversibility is also accompanied by substantial capacity retention at each of these rates(Fig. S3b and Fig. S4b).

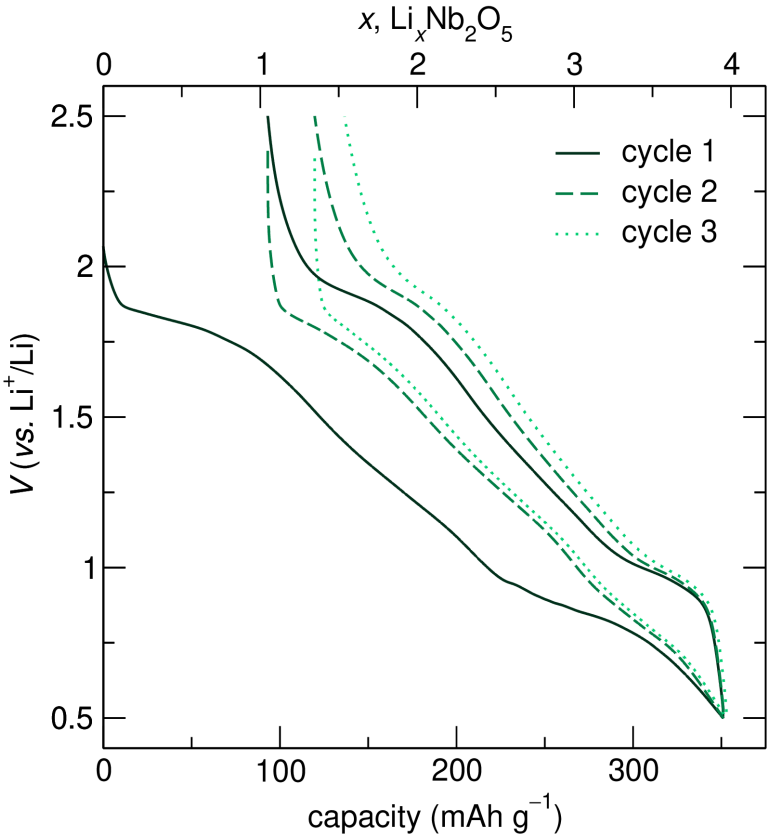

Figure S2: Galvanostatic cycling data for $R-Nb_2O_5$ as a loose powder cathode (mixed with SuperP) in a Swagelok cell against Li metal with a lower potential limit of 0.5 V. and an upper potential limit of 2.5 V.

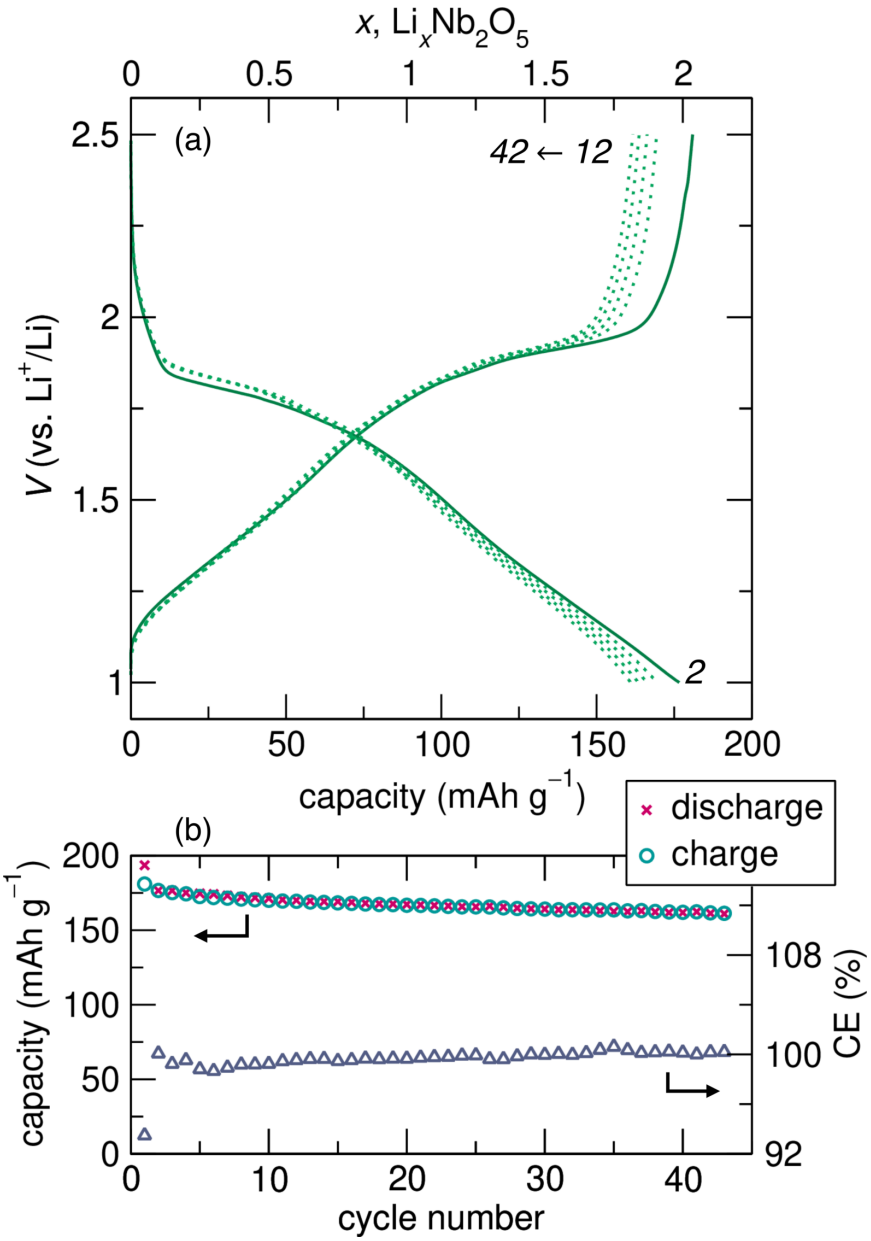

Figure S3: Galvanostatic cycling data of $R{-}Nb_2O_5$ in a coin cell cycled at a rate of $C/10$. (a) Discharge and charge profiles for cycles 2, 12, 22, 32, and 42; (b) capacity and Coulombic efficiency per cycle for 45 cycles. Cycle 1 has been excluded for clarity to emphasize the reversible cycling; as at $C/20$, the first discharge has a distinct profile shape relative to subsequent cycles.

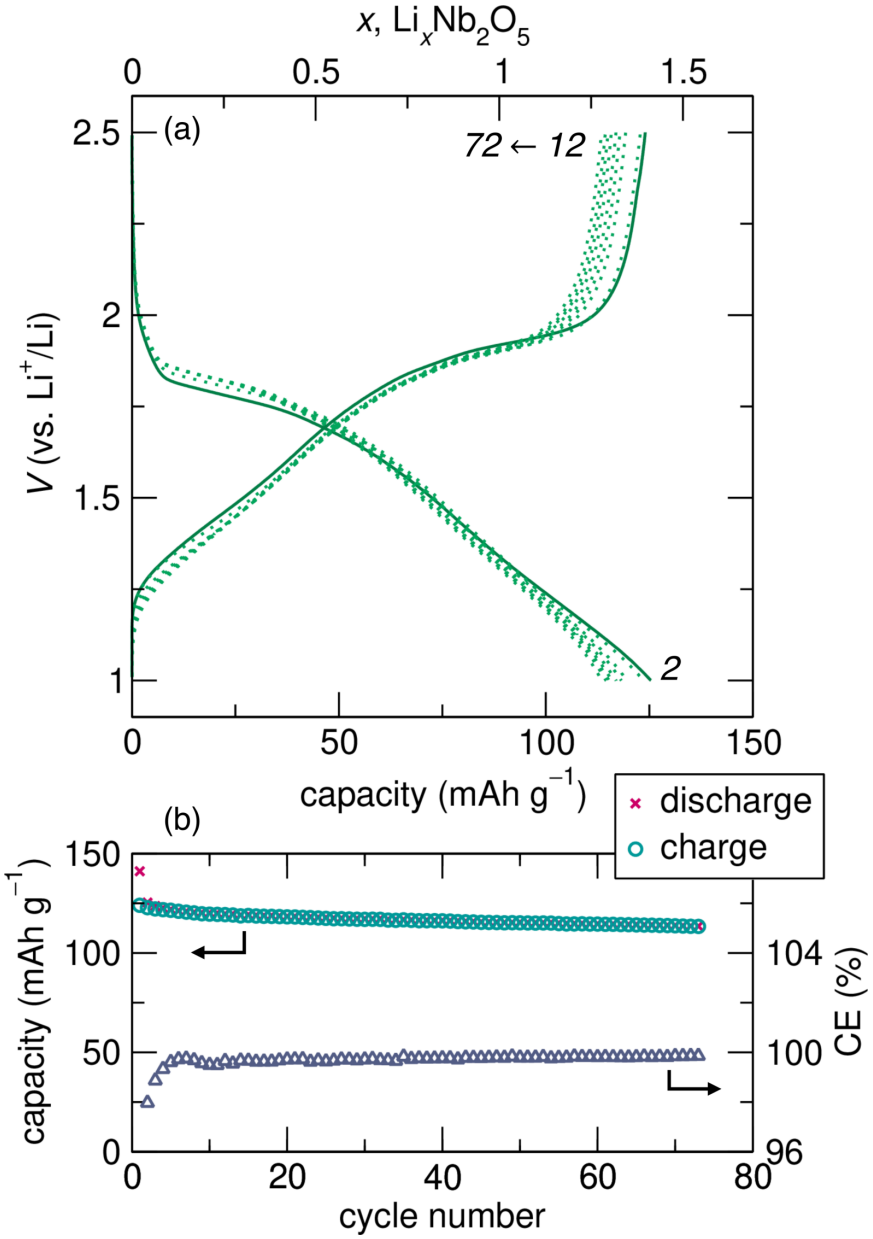

Figure S4: Galvanostatic cycling data of $R{-}Nb_2O_5$ in a coin cell cycled at a rate of $1C$. (a) Discharge and charge profiles for cycles 2, 12, 22, 32, 42, 52, 62, and 72; (b) capacity and Coulombic efficiency per cycle for 72 cycles. Cycle 1 has been excluded for clarity to emphasize the reversible cycling; as at $C/20$, the first discharge has a distinct profile shape relative to subsequent cycles.

References

(1) Coelho, A. A. TOPAS and TOPAS-Academic: An Optimization Program Integrating Computer Algebra and Crystallographic Objects Written in C++. *J. Appl. Crystallogr.* **2018**, *51*, 210–218.